CONSISTENCY CHECK OF DROP SIZE DISTRIBUTION IN RAIN RETRIEVALS WITH A COMBINATION OF TRMM MICROWAVE IMAGER AND PRECIPITATION RADAR OBSERVATIONS

Shoichi Shige[(1)]*, Toshio Iguchi[(2)], Shuji Shimizu[(3)], Nobuhiro Takahashi[(2)],
Toshiaki Kozu[(3)] and Ken'ichi Okamoto[(4)]

(1) Department of Aerospace Engineering, Osaka Prefecture University, Sakai, Japan
(2) National Institute of Information and Communications Technology (NICT), Koganei, Tokyo, Japan
(3) JAXA/Earth Observation Research Center, Tokyo, Japan
(4) Department of Electronic and Control systems Engineering, Shimane University, Matsue, Japan

1. INTRODUCTION

The TRMM Microwave Imager (TMI) and Precipitation Radar (PR) have been providing distribution of rainfall throughout the Tropics and contributed significantly towards reducing uncertainty in satellite estimates of rainfall. Although differences in global averaged rainfall between the two sensors have been reducing, regional and seasonal differences still exist (Berg et al., 2002). Possible error sources static model assumptions involved with individual retrieval algorithm. For TMI rain retrieval (Kummerow et al., 1996), the database of cloud/radiative model simulations is very important. On the other hand, for PR rain algorithm (Iguchi et al., 2000), the appropriate selection of drop size distribution (DSD) is very important because observed radar reflectivities Z depend strongly upon the size of water drops.

Here, the consistency in observed and simulated brightness temperature is investigated, where the simulated brightness temperature are derived from PR precipitation profiles, similar to Viltard et al. (2000), but for a case over the South China Sea Monsoon Experiment (SCSMEX). We examine whether or not the DSD model assumed by the PR algorithm produces good or poor agreement between observed and simulated brightness temperature.

2. DATA DESCRIPTIONS

We use two of TRMM standard data products, referenced as PR rain rate/PR-corrected reflectivity (2A25) and TMI brightness temperature (1B11). Both standard products here are version 5. The results reported in this short paper are based on a scene observed on a subset of orbit 2719 on 19 May 1998 from the SCSMEX region.

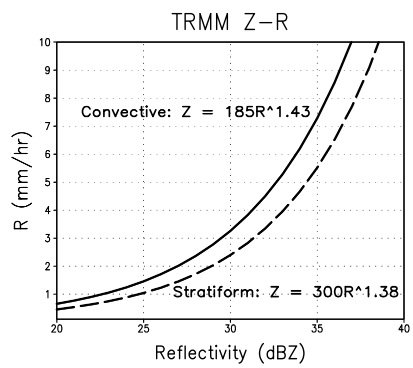

Figure 1: TRMM Z-R

Here we introduce a brief summary of Z-R relations, or, equivalently, the drop size distribution (DSD) for 2A25. The "globally" averaged Z-R relation used in version 5 of 2A25 are as follows

$$Z = 185R^{1.43}\text{(convective)}, \qquad (1)$$

and

$$Z = 300R^{1.38}\text{(stratiform)}. \qquad (2)$$

The Z-R relations are obtained from a collection of Z-R relations measured near the oceanic from widely distributed locations around the world (Kozu et al., 1999). As shown in Fig. 1, the same Z translates to R smaller in stratiform compared to convective rainfall. This is because the presence of a few very large drop (formed from the melting large aggregates) in the stratiform drop spectra increases the radar reflectivity much more than it increases the rain volume (Rosenfeld and Ulbrich, 2003).

*Corresponding author address: Dr. Shoichi Shige, Department of Space Engineering, Osaka Prefecture University, 1-1 Gakuen-cho, Sakai, Osaka, 599-8531 Japan; e-mail: shige@aero.osakafu-u.ac.jp

For each model, the Z-R relationships are converted into an $N_0 - \Lambda$ relationship, where N_0 and Λ are parameters in the size distribution:

$$N(D) = N_0 D^{\mu} exp(-\Lambda D). \tag{3}$$

Here, D is drop diameter. It is assumed that μ is constant and taken a value of $\mu = 3$.

3. RESULTS AND DISCUSSIONS

In this study, the radiative transfer model (RTM) developed by Liu (1998) is used to calculate brightness temperatures. TMI brightness temperature at 10.65 GHz where absorption is the dominant effect are less sensitive to DSD or the effect of ice scattering. Because it is very difficult ice phase precipitation derived from PR data, we focus on brightness temperature at 10.65 GHz.

3.1. Sensitivity tests

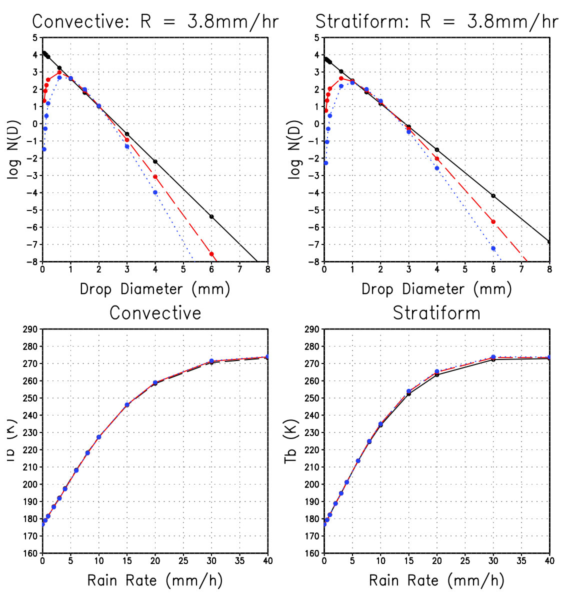

Figure 2: Drop Size distribution for μ = 0 (solid), 3 (dashed), and 6 (dotted) derived TRMM PR Z-R relations (upper panels) and the 10.65 GHz V-polarization brightness temperature for homogeneous rain with μ = 0 (black), 3 (red), and 6 (blue).

To understand the effects of the DSD model, we first calculate brightness temperatures for an atmosphere with homogeneous rain extending from the surface to 3.0 km, with different values of μ (= 0, 3, 6) in Eq. (3), for convective and stratiform rain, respectively. Even though different values of μ give seemingly different size distribution as shown in the upper panels of Fig. 2, the selection of μ does not affect the 10.65 GHz vertically polarized brightness temperatures as shown in the bottom panels of Fig. 2. This is because the selection of μ does not affect water content. Hereafter, μ is taken a value of $\mu = 3$, following the PR DSD model.

3.2. Brightness temperature simulations

As input data for the RTM, we use the atmospheric temperature, surface wind and specific humidity from SCSMEX NESA (Northern Enhanced Sounding Array) averaged dataset (Johnson and Ciesielski, 2002). Sea surface temperature data derived from the TMI data (Shibata et al., 1999) is also used.

To take into account the antenna pattern, a weighted average of the brightness temperature at the radar resolution is performed as follows:

$$Y = \sum_j g_j X \bigg/ \sum_j g_j \tag{4}$$

where

$$g_j = exp\Big[-ln(2)\Big(\Big(\frac{x}{\sigma_x}\Big)^2 + \Big(\frac{y}{\sigma_y}\Big)^2\Big)\Big] \tag{5}$$

is a Gaussian weighting factor. Here x and y are the distance in kilometers between a PR footprint (index by j) and the specified TMI footprint, in the cross-track and down-track directions, respectively. The summation Eq.(4) is over all PR footprints within $2.5(x^2/\sigma_x^2 + y^2/\sigma_y^2)^{0.5}$ of the TMI footprint where σ_x = 36.8 km and σ_y = 63.2 km. Here X is the simulated TB from PR.

Figure 3 illustrates the brightness temperature simulations that the antenna patterns affects. Although the general spatial patterns are very well reproduced, the lack of emission at 10 GHz-V is obvious. This result is consistent with the results of Viltard et al. (2000) for a case in the central Pacific. Following Olson et al. (2001b), a weighted average of PR-derived convective and stratiform area fractions in the neighborhood of a given TMI footprint are performed by substituting the PRC$_j$ and PRS$_j$ for X in Eq. 4, respectively. Here

$$\text{PRC}_j = \begin{cases} 1, & \text{convective PR classification} \\ 0, & \text{otherwise} \end{cases} \tag{6}$$

and

$$\text{PRS}_j = \begin{cases} 1, & \text{stratiform PR classification} \\ 0, & \text{otherwise} \end{cases} \tag{7}$$

are based upon Awaka et al. (1998) PR classification, respectively. One may notice that the regions with lack of emission roughly correspond to the regions of large convective area fractions.

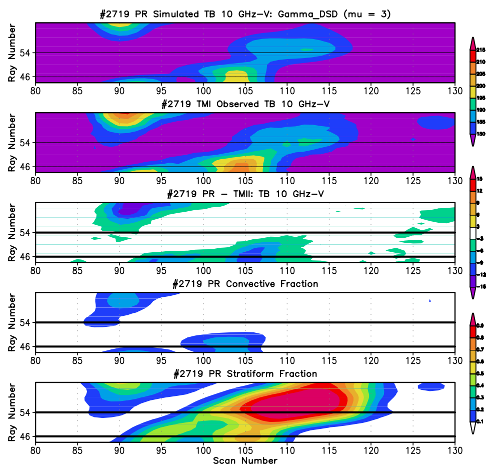

Figure 3: Imagery of mesoscale systems occurring over the SCSMEX region on 19 May 1998, (a) Simulated brightness temperatures for 10 GHz-V obtained from PR rain profiles, (b) TMI observed brightness temperatures for 10 GHz-V, (c) simulated brightness temperatures minus observed brightness temperatures, (d) PR-derived convective area fractions at a resolution comparable to the TMI, and (d) PR-derived stratiform area fractions at a resolution comparable to the TMI.

Figure 4 illustrates the height-zonal cross sections of PR observed radar reflectivities for ray number of 46 where the lack of emission is noticed in Fig. 3. For more direct comparison, a weighted average of the PR radar reflectivities in the neighborhood of a given TMI footprint is performed, by substituting the PR radar reflectivities for X_j in Eq. 4. The regions with lack of emission roughly correspond to those of large PR-derived stratiform area fractions. These region of large stratiform area fractions are very close to the region with large convective area fractions.

In contrast, the region of large PR-derived stratiform area fractions in ray number of 54 shows very good agreement between simulated and observed TBs (Fig. 3). The radar reflectivities in this region has typical stratiform characteristics because they still shows the bright band even if a weighted average is performed.

Part of poor agreement between simulated and observed TBs in the stratiform region near the convective region may be due to selection of the Z-R relation in 2A25. In convective-stratiform classification, the same Z translates to R smaller in stratiform compared to convective rainfall (Eqs. (1), (2)). This is based on the presence of a few large drops in the stratiform drop spectra. The dominant growth processes of stratiform precipitation are vapor deposition onto existing ice particles and the collection of snow generated by the mesoscale updraft that develops in the upper levels in the stratiform regions (Rosenfeld and Ulbrich, 2003). In the stratiform region near the convective region, the passage of the particles through the region of mesoscale updraft may be not enough for the growth of large drops. Hence, the selection of the Z-R relation, or, equivalently the DSD for stratiform (Eq. (2)) may be inappropriate.

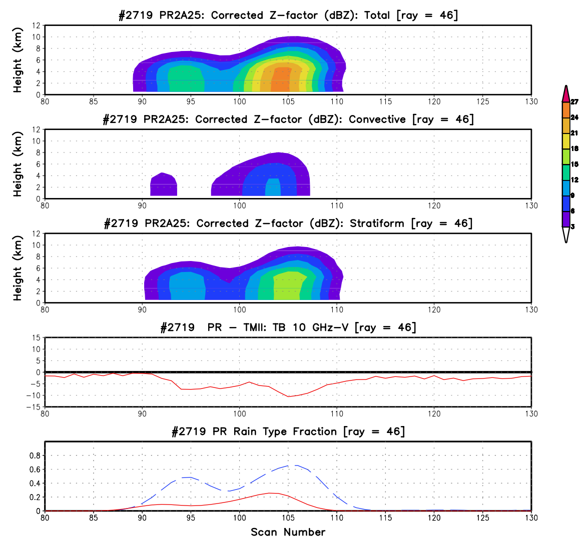

Figure 4: Vertical cross section of PR observed radar reflectivity at a resolution comparable to the TMI for ray number of 46. (a) total, (b) convective, and (c) stratiform. (d) Simulated brightness temperatures minus observed brightness temperatures, and (e) PR-derived convective (solid) and stratiform (dashed) area fractions at a resolution comparable to the TMI.

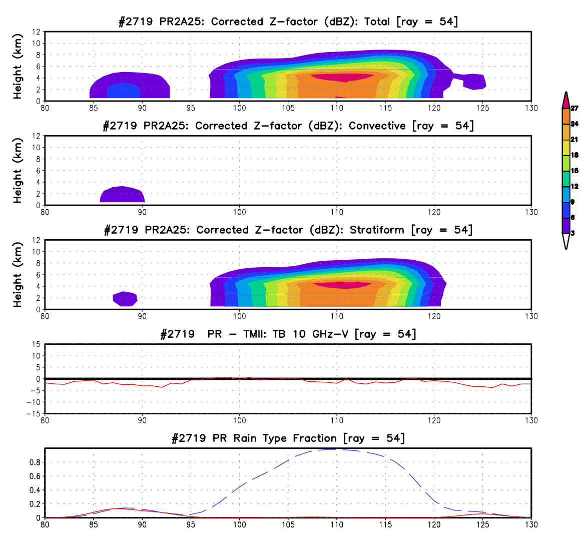

Figure 5: Same as Fig. 4, but for ray number of 54.

4. SUMMARY AND FUTURE WORKS

In this study, the consistency in observed and simulated brightness temperature (TB) is investigated, where the simulated TB is derived from PR precipitation profiles, similar to Viltard et al. (2000), but for a case over the South China Sea Monsoon Experiment (SCSMEX).

Simulated TB is lower than observed one in the stratiform region near the convective region, especially the region of a stratiform subcategory with no bright band. This may be due to the selection of Z-R relationship in PR2A25 where the same Z translates to R smaller in stratiform compared to convective rainfall. The stratiform Z-R relation assuming large rain drops melted from large aggregates may be inappropriate for the stratiform region near the convective region.

Finally, it should be noted conclusions are tentative. The dependence of rain rate on the altitude was not yet taken into account in the RTM calculations. The rain rate at different altitude is corrected for the difference of the terminal velocity with altitude in the 2A25 algorithm. This is because the rain rate is a function of the raindrop fall speeds, which, in turn, are determined by raindrop sizes and air density (Foote and du Toit, 1969). This dependence of rain rate on the altitude will be taken into account. The impact of melting particles on radiances also needs to be considered (Olson et al., 2001a). As mean size distributions of raindrops are measured in SCSMEX by dual-polarized radar (Bringi et al., 2003), conclusions might be verified more directly.

Acknowledgement This study is supported by the fund of Japan Science and Technology Corporation - Core Research for Evolution Science and Technology (CREST). We wish to thank Prof. G. Liu of Florida State University for providing his radiative transfer model. We also thank Dr. K. Aonashi for his kind guidance on using the radiative transfer model.

REFERENCES

Awaka, J., T. Iguchi, and K. Okamoto: 1998, Early results on rain type classification by the Trpopical Rainfall Measuring Mission (TRMM) precipitation radar. *Proc. 8th URSI Commision F Open Symp.*, URSI, Aveiro, Portugal, 143–146.

Berg, W. K., C. Kummerow, and C. A. Morales: 2002, Differences between east and west pacific rainfall systems. *J. of Climate*, **15**, 3659–3672.

Bringi, V. N., V. Chandrasekar, H. Hubbert, E. Gorgucci, W. L. Randeu, and M. Schoenhuber: 2003, Rindrop size distribution in different climate regimes from disdrometer and dual-polarized radar analysis. *J. Atmos. Sci.*, **60**, 354–365.

Foote, G. B. and P. S. du Toit: 1969, Terminal velocity of raindrops aloft. *J. Appl. Meteor.*, **8**, 249–253.

Iguchi, T., T. Kozu, R. Meneghini, J. Awaka, and K. Okamoto: 2000, Rain-profiling algorithm for the TRMM precipitation radar. *J. Appl. Meteor.*, **39**, 2038–2052.

Johnson, R. H. and P. E. Ciesielski: 2002, Characteristics of the 1998 summer monsoon onset over the northern South China Sea. *J. Meteor. Soc. Japan*, **80**, 561–578.

Kozu, T., T. Iguchi, K. Shimizu, and N. Kawagishi: 1999, Estimation of rain drop size distribution parameters using statistical relations between multiparameter rainfall remote sensing data. *Preprints, 29th Int. Conf. on Radar Meteorology*, Amer. Meteor. Soc., Montreal, Quebec, Canada, 689–692.

Kummerow, C., W. S. Olson, and L. Giglio: 1996, A simplified scheme for obtaining precipitation and vertical hydrometer profiles from passive microwave sensors. *IEEE Trans. Geosci. Remote Sens.*, **34**, 1213–1232.

Liu, G.: 1998, A fast and accurate model for microwave radiance calculations. *J. Meteor. Soc. Japan*, **76**, 335–343.

Olson, W. S., P. Bauer, C. D. Kummerow, Y. Hong, and W.-K. Tao: 2001a, A melting-layer model for passive/active microwave remote sensing applications. Part II: Simulation of TRMM observations. *J. Appl. Meteor.*, **40**, 1164–1179.

Olson, W. S., Y. Hong, C. D. Kummerow, and J. Turk: 2001b, A texture-polarization method for estimating convective-stratiform precipitation area coverage from passive microwave radiometer data. *J. Appl. Meteor.*, **40**, 1577–1591.

Rosenfeld, D. and C. W. Ulbrich: 2003, Cloud microphysical properties, process, and rainfall estimation opportunities. *Radar and Atmospheric Science: A Collection of Essays in Honor of David Atlas*, Amer. Meteor. Soc., number 52 in Meteor. Monogr., 237–258.

Shibata, A., K. Imaoka, K. Kachi, and H. Murakami: 1999, SST observation by TRMM Microwave Imager aboard Tropical Rainfall Measuring Mission. *Umi no Kenkyu*, **8**, (In Japanese).

Viltard, N., C. Kummerow, W. S. Olson, and Y. Hong: 2000, Combined use of the radar and radiometer of trmm to estimate the influence of drop size distibution on rain retrievals. *J. Appl. Meteor.*, **39**, 2103–2114.